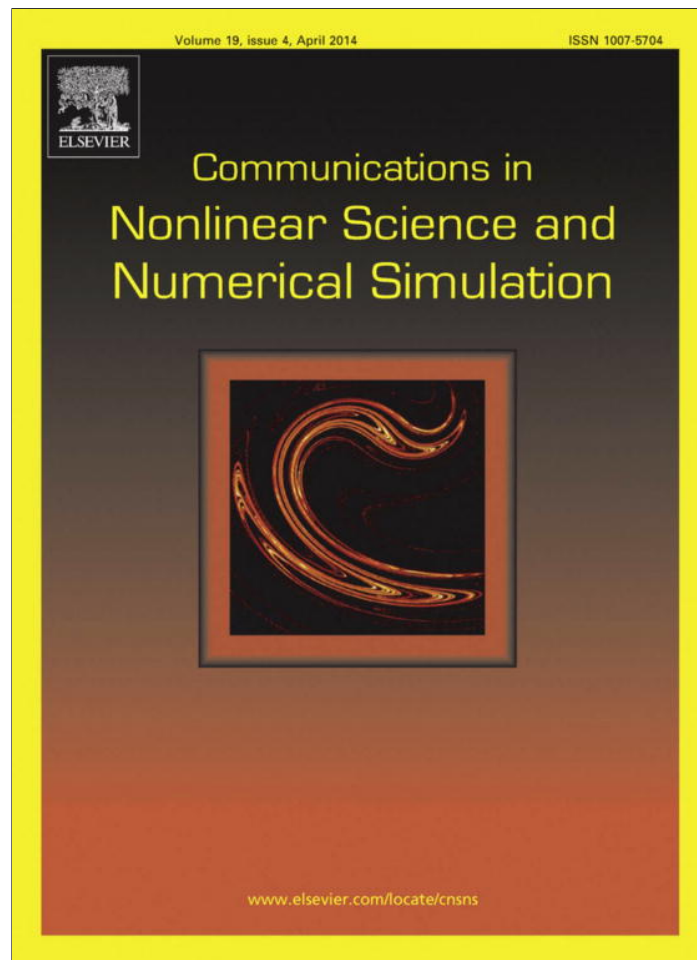


Provided for non-commercial research and education use.
Not for reproduction, distribution or commercial use.



This article appeared in a journal published by Elsevier. The attached copy is furnished to the author for internal non-commercial research and education use, including for instruction at the authors institution and sharing with colleagues.

Other uses, including reproduction and distribution, or selling or licensing copies, or posting to personal, institutional or third party websites are prohibited.

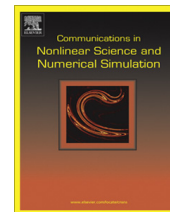
In most cases authors are permitted to post their version of the article (e.g. in Word or Tex form) to their personal website or institutional repository. Authors requiring further information regarding Elsevier's archiving and manuscript policies are encouraged to visit:

<http://www.elsevier.com/authorsrights>



Contents lists available at ScienceDirect

Commun Nonlinear Sci Numer Simulat

journal homepage: www.elsevier.com/locate/cnsns

Nonlinear dynamics of internet congestion control: A frequency-domain approach

Franco S. Gentile^{a,b,*}, Jorge L. Moiola^{a,c}, Eduardo E. Paolini^{a,c}^a Instituto de Investigaciones en Ingeniería Eléctrica – IIIE (UNS-CONICET), Argentina^b Departamento de Matemática, Universidad Nacional del Sur, B8000CPB Bahía Blanca, Argentina^c Departamento de Ingeniería Eléctrica y de Computadoras, Universidad Nacional del Sur, B8000CPB Bahía Blanca, Argentina

ARTICLE INFO

Article history:

Received 30 November 2012

Accepted 9 August 2013

Available online 23 August 2013

Keywords:

Time-delay systems

Frequency-domain approach

Internet congestion control

Multiple oscillations

ABSTRACT

In this paper a fluid-flow model for TCP congestion avoidance combined with different AQM schemes is analyzed. The conditions for the appearance of Hopf bifurcations are stated analytically using frequency-domain techniques. The proposed methodology allows the characterization of the emerging periodic orbits, providing approximations of their amplitude and frequency. In addition, multiple oscillations and limit cycle bifurcations are found via numerical tools.

© 2013 Elsevier B.V. All rights reserved.

1. Introduction

Nowadays internet congestion is a serious and challenging problem, which arises when a resource becomes overloaded, causing an overflow on the transmission channels. Then, some pieces (packets) of data are lost, and the whole system may experience a performance degradation. This inconvenience resulted in intensive research of congestion control algorithms. These control tactics rely on two key mechanisms interacting in a communication development: Transmission Control Protocol (TCP) and Active Queue Management (AQM). Roughly speaking, TCP is an end-to-end protocol that sets the transmission rate of sources by a window adjustment policy. This process relies on the feedback achieved through the acknowledgment (ACK) packets sent back by receivers, which allow the sources to estimate the congestion level of the involved links. On the other hand, AQM consists of the implementation of an inner feedback loop, generating a control signal (generally a marking probability) depending on the amount of data queued in the router. That probability raises as the queue grows, thus some packets are marked to be discarded before the queue becomes full, early preventing the congestion.

The main purpose of an internet congestion control algorithm is to guarantee the stability of the system, i.e., the flow of information through its links should tend towards a stationary value, preferably exploiting most of the link capacity. However, the traffic around the network and the network itself is in fact always changing. Under these typical variations, some schemes exhibit poor performance, and may even become unstable. Frequently the stability loss is followed by the onset of oscillating regimes, leading to bad communication development and underutilization of links. This change in the system's behavior is provoked by a mechanism known as Hopf bifurcation, which is responsible for the appearance of oscillations in several engineering systems. In the particular context of internet congestion control, this phenomenon has been studied

* Corresponding author at: Departamento de Matemática, Universidad Nacional del Sur, B8000CPB Bahía Blanca, Argentina. Tel.: +54 291 4595101; fax: +54 291 4595154.

E-mail address: fsgentile@gmail.com (F.S. Gentile).

by several authors, for example [1–4] to mention only a few. One question is why those systems are so prone to oscillate. Immediately, two main characteristics of TCP get relevant. Firstly, the nonlinear law proposed for updating the window size, i.e., AIMD (*additive increase – multiplicative decrease*). Secondly, the inherent delayed feedback accomplished when a packet is sent to the receiver and the corresponding ACK returns to the source. The time elapsed between the packet sending and the ACK arriving is called *round trip time* (RTT), and it strongly favors the onset of instabilities [4].

Through this paper, we shall consider a TCP fluid-flow model developed in [5]. This model has been widely used in the literature (see, for example [3,2,4,6]) and it has been formulated as a delay-differential equation (DDE), where the involved delay is in fact the RTT. That model will be combined with three different AQM schemes, say the well-known RED (*random early detection*), and the proportional (P) and proportional-integral (PI) controllers proposed in [6]. Our purpose is to analyze the nonlinear behavior of the resulting system from the perspective of bifurcation theory. As emphasized in [7], this viewpoint is very helpful to better understand the TCP/AQM mechanisms better.

Novel results about the nonlinear dynamics of those systems are stated analytically, through the frequency-domain (FD) approach [8–10], which provides an alternative tool for the stability analysis and the study of local bifurcations. In the case of DDEs, the main advantage of the FD approach is the avoidance of dealing with a transcendental equation [11]. Instead, as stated in the Graphical Hopf Bifurcation Theorem [8], we study a curve in the complex plane (Nyquist plot) determined by a characteristic function [8,10]. In addition, the proposed technique allows the computation of the amplitude, frequency and stability of the periodic solutions emanating from Hopf bifurcations. We also use the package DDE-BIFTOOL [12] to extend our results detecting nonlocal bifurcations. Multiple fold bifurcations of cycles appear as a distinctive feature in the periodic branch continuations. This result has not been previously reported in the technical literature of internet congestion control.

2. Preliminaries: the frequency-domain (FD) approach for time-delay systems

Let us consider an autonomous, DDE of the form

$$\begin{cases} \dot{\mathbf{x}}(t) &= A(\mu)\mathbf{x}(t) + B(\mu)\mathbf{g}(\mathbf{y}(t), \mathbf{y}(t - \tau); \mu), \\ \mathbf{y}(t) &= -C(\mu)\mathbf{x}(t), \end{cases} \quad (1)$$

where $\mathbf{x} \in \mathbb{R}^n$, $A(\mu) \in \mathbb{R}^{n \times n}$, $B(\mu) \in \mathbb{R}^{n \times p}$, $C(\mu) \in \mathbb{R}^{m \times n}$, μ is a vector of parameters, $\tau > 0$ is a constant time-delay and $\mathbf{g} : \mathcal{C} \times \mathbb{R} \rightarrow \mathbb{R}^p$ is a smooth nonlinear function, where $\mathcal{C} := \mathcal{C}([-\tau, 0], \mathbb{R}^m)$ denotes the Banach space of all continuous functions mapping the interval $[-\tau, 0]$ into \mathbb{R}^m , equipped with the norm $\|\phi\|_{\mathcal{C}} = \sup_{-\tau \leq \zeta \leq 0} |\phi(\zeta)|$. System (1) can be represented by the feedback scheme shown in Fig. 1(a), by taking $G(s; \mu) = C(\mu)[sI_n - A(\mu)]^{-1}B(\mu)$, where s is the complex variable of the Laplace transform and I_n is the $n \times n$ identity matrix. Since the system is autonomous, input $\mathbf{d}(t)$ is identically zero. The delay can be absorbed into the linear block through a simple manipulation (see [11]). Let

$$F(e^{-s\tau}) := \begin{pmatrix} I_m \\ I_m e^{-s\tau} \end{pmatrix}, \quad \mathbf{y}^*(t) := \begin{pmatrix} \mathbf{y}(t) \\ \mathbf{y}(t - \tau) \end{pmatrix},$$

then we can represent the system as shown in Fig. 1(b), where the linear part becomes $G^*(s; \mu) := F(e^{-s\tau})G(s; \mu)$ and $\mathbf{y}^*(t)$ represents an extended output. By assuming that $A(\mu)$ is invertible, the equilibrium points $\hat{\mathbf{y}}^*$ can be found by solving

$$G^*(0; \mu)\mathbf{g}(\hat{\mathbf{y}}^*, \hat{\mathbf{y}}^*; \mu) = -\hat{\mathbf{y}}^*. \quad (2)$$

Finally, we can linearize the nonlinear function at equilibrium computing the Jacobian

$$J(\mu) = [\partial \mathbf{g}(\cdot) / \partial \mathbf{y}(t) \quad \partial \mathbf{g}(\cdot) / \partial \mathbf{y}(t - \tau)]|_{(\mathbf{y}(t), \mathbf{y}(t - \tau)) = (\hat{\mathbf{y}}, \hat{\mathbf{y}})}.$$

The procedure for detecting a bifurcation in the FD setting is as follows. Let $s = i\omega$ in the matrix $G^*(s; \mu)$, and consider the following result given in [8,10]:

Lemma 1. *If a given solution of the characteristic equation of the nonlinear system (1), in the time domain, assumes a purely imaginary value $i\omega_0$ at a particular value $\mu = \mu_0$, then an eigenvalue of matrix $G^*(s; \mu_0)J(\mu_0)$ in the FD must assume the value $-1 + i0$ for $(s; \mu) = (i\omega_0; \mu_0)$.*

The eigenvalues or characteristic functions $\lambda(s; \mu)$ of $G^*(s; \mu)J(\mu)$ satisfy the frequency-domain version of the characteristic equation given by

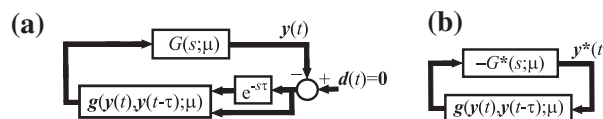


Fig. 1. (a) Block representation of system (1). (b) Equivalent block representation with the delay absorbed into the linear part.

$$|\lambda I_{2m} - G^*(s; \mu)J(\mu)| = \lambda^{2m} + a_{2m-1}(s, e^{-s\tau}; \mu)\lambda^{2m-1} + \dots + a_0(s, e^{-s\tau}; \mu) = 0. \tag{3}$$

At first glance, it is possible to think that the definition of the augmented matrix $G^*(s; \mu)$ is not convenient, because the number of characteristic functions in (3) rises immediately from m to $2m$. However, from the definition of $G^*(s; \mu)$, the maximum possible rank of that matrix is actually m , and as consequence at least m of the $2m$ eigenfunctions are identically zero. In addition, there are infinitely many ways of representing the system $\mathbf{x}(t) = \mathbf{f}(\mathbf{x}(t), \mathbf{x}(t - \tau); \mu)$ in the form (1) choosing proper matrices $A(\mu)$, $B(\mu)$ and $C(\mu)$ (such a selection of matrices is called a realization [10]). Normally, it is possible to take a realization leading to $J(\mu)$ with rank one, as we will show in the examples. In this case, the augmented system has only one characteristic function that is not identically zero. Perhaps this fact manifests one of the advantages of the FD methodology: the drastic dimensional reduction of the problem when compared to the time-domain analogue. We deal with a few (luckily, just one) characteristic functions instead of the infinite spectrum associated with corresponding time-domain formulation.

Suppose that for $\mu = \mu_0$, there exists a simple root $\hat{\lambda}(s; \mu)$ of (3) which takes the value $-1 + i0$ for a given $s = i\omega_0$. The geometrical locus of $\hat{\lambda}(i\omega; \mu)$ describes a curve (Nyquist locus) parameterized by the frequency ω . Particularly, for $\mu = \mu_0$ this curve crosses the point $-1 + i0$ at $\omega = \omega_0$. If $\omega_0 = 0$ ($\omega_0 \neq 0$) there is a static (dynamic) bifurcation taking place for the critical value $\mu = \mu_0$. We may wonder what kind of behavior the system has for parameter values near this critical one. More precisely, focusing on Hopf bifurcations, it is desirable to develop the characteristics of the emerging periodic solutions. On this regard, let μ vary slightly from μ_0 and compute the auxiliary vector

$$\xi(\omega; \mu) = -\mathbf{u}^T G^*(i\omega; \mu) \mathbf{p}(i\omega; \mu) / (\mathbf{u}^T \mathbf{v}), \tag{4}$$

where \mathbf{u} and \mathbf{v} are the left and right eigenvectors of $G^*(i\omega; \mu)J(\mu)$ associated to $\hat{\lambda}(i\omega; \mu)$, and

$$\mathbf{p}(i\omega; \mu) = Q\mathbf{V}_{02} + \frac{1}{2}Q\bar{\mathbf{V}}_{22} + \frac{1}{8}L\bar{\mathbf{v}}, \tag{5}$$

where \mathbf{V}_{02} and \mathbf{V}_{22} are proportional to the zero and second coefficients in the Fourier representation of the output $\mathbf{y}^*(t)$, and they are given by

$$\mathbf{V}_{02} = -\frac{1}{4}H^*(0; \mu)Q\bar{\mathbf{v}}, \quad \mathbf{V}_{22} = -\frac{1}{4}H^*(i2\omega; \mu)Q\mathbf{v}, \tag{6}$$

where $H^*(s; \mu) := [I_{2m} + G^*(s; \mu)J(\mu)]^{-1}G^*(s; \mu)$. Matrices $Q := (q_{jk})$ and $L := (\ell_{jk})$ (of dimensions $p \times 2m$) are computed as

$$q_{jk} = \sum_{i=1}^{2m} \frac{\partial^2 g_j}{\partial y_i \partial y_k} \Big|_{\hat{\mathbf{y}}} v_i, \quad \ell_{jk} = \sum_{i=1}^{2m} \sum_{\ell=1}^{2m} \frac{\partial^3 g_j}{\partial y_i \partial y_\ell \partial y_k} \Big|_{\hat{\mathbf{y}}} v_i v_\ell, \tag{7}$$

where g_j and v_j mean the j -component of $\mathbf{g}(\cdot)$ and \mathbf{v} , respectively. Let us consider the following result given in [8,10], which for reader's convenience is briefly stated as follows

Theorem 1. Graphical Hopf Bifurcation Theorem: Suppose that when ω varies, the vector $\xi(\omega; \mu) \neq 0$, and that the half line starting from $-1 + i0$ and pointing to the direction parallel to that of $\xi(\omega; \mu)$, first intersects the locus of $\hat{\lambda}(i\omega; \mu)$ at the point

$$P = \hat{\lambda}(i\tilde{\omega}; \mu) = -1 + \xi(\tilde{\omega}; \mu)\theta^2, \tag{8}$$

where the constant $\theta = \theta(\mu)$ is equal or greater than 0. Suppose, furthermore, that the above intersection is transversal, i.e., $\hat{\lambda}(i\tilde{\omega}; \mu)$ and $\xi(\tilde{\omega}; \mu)$ are not parallel. Then:

1. The nonlinear system (1) has a limit cycle which is unique in a ball of radius $\mathcal{O}(1)$ centered at $\hat{\mathbf{y}}^*$.
2. If the total number of anticlockwise encirclements of the point $P + \delta\xi(\tilde{\omega}; \mu)$, for a small enough δ , is equal to the number of poles of $\hat{\lambda}(s; \mu)$ with positive real parts, then the limit cycle is stable.

The positive quantity θ is a measure of the amplitude and $\tilde{\omega}$ is the approximate frequency of the periodic solution, which is represented by the second-order Fourier expansion

$$\mathbf{y}^*(t) \simeq \hat{\mathbf{y}}^* + \Re \left\{ \sum_{k=0}^2 \mathcal{Y}^k e^{ik\tilde{\omega}t} \right\}, \tag{9}$$

where $\Re(\cdot)$ means the real part of a complex quantity and coefficients \mathcal{Y}^k are given by

$$\mathcal{Y}^0 = \theta(\mu)^2 \mathbf{V}_{02}, \quad \mathcal{Y}^1 = \theta(\mu) \mathbf{v}, \quad \mathcal{Y}^2 = \theta(\mu)^2 \mathbf{V}_{22}. \tag{10}$$

The only open question is how to find the solution pair $(\tilde{\omega}, \theta)$ that solves (8). This can be accomplished by an iterative process, starting from ω_0 , the frequency at which $\hat{\lambda}(i\omega; \mu_0)$ crosses the $-1 + i0$ point. If μ is close enough to μ_0 , the true frequency $\tilde{\omega}$ remains close to ω_0 [8]. Then, we follow the steps below

$$\begin{aligned}
 \text{(Step 1)} \quad & \widehat{\lambda}(i\omega_1; \mu) = -1 + \xi(\omega_0; \mu)\theta_1^2, \\
 \text{(Step 2)} \quad & \widehat{\lambda}(i\omega_2; \mu) = -1 + \xi(\omega_1; \mu)\theta_2^2, \\
 & \vdots \\
 \text{(Step } N) \quad & \widehat{\lambda}(i\omega_N; \mu) = -1 + \xi(\omega_{N-1}; \mu)\theta_N^2,
 \end{aligned} \tag{11}$$

taking N large enough so that $|\omega_N - \omega_{N-1}| < \epsilon$, with ϵ very small. Finally, we assign $\tilde{\omega} := \omega_N$ and $\theta := \theta_N$. In addition, the stability of the orbit at the onset of the Hopf bifurcation can be determined algebraically by computing the *curvature coefficient*, which is given by

$$\sigma_0 = -\Re \left\{ \frac{\mathbf{u}^T G^*(i\omega_0; \mu) \mathbf{p}(\omega_0; \mu)}{\mathbf{u}^T G^{*'}(i\omega_0; \mu) \mathbf{J}(\mu) \mathbf{v}} \right\}, \tag{12}$$

where $G^{*'}(i\omega; \mu) := \partial G^*(s; \mu) / \partial s|_{s=i\omega}$. Then, if σ_0 is *negative (positive)*, the Hopf bifurcation is *supercritical (subcritical)*, and a *stable (unstable)* periodic solution exists when the equilibrium is *unstable (stable)*.

3. Model description

Through this paper, we will consider the dynamic model developed in [5], which is described by the following nonlinear DDE

$$\begin{cases} \dot{W}(t) = \frac{1}{R(t)} - \frac{1}{2} \frac{W(t)W(t-R(t))}{R(t-R(t))} P(t-R(t)), \\ \dot{Q}(t) = \frac{N(t)W(t)}{R(t)} - C_l(t), \end{cases} \tag{13}$$

where $W(t)$ is the average TCP window size (packets), $Q(t)$ is the average queue length (packets), $N(t)$ is a load factor (number of TCP sessions), $C_l(t)$ is the link capacity (packets/s), $R(t)$ is the RTT (s) and $P(t)$ is the probability of packet mark. The RTT involves the propagation delay T_p and the queuing time, i.e.,

$$R(t) = Q(t)/C_l(t) + T_p. \tag{14}$$

System (13) has a state-dependent delay, and therefore the analytical study is a challenging task. A frequently simplifying assumption is to suppose that the link capacity and the number of TCP sessions are constants, i.e., $C_l(t) = C_l$ and $N(t) = N$. The equilibrium satisfies $(\widehat{W}(t), \widehat{Q}(t)) = (0, 0)$, yielding the following equations for the stationary values:

$$\begin{cases} \widehat{W}^2 \widehat{P} = 2, \\ N \widehat{W} = C_l \widehat{R}, \quad \widehat{R} = \widehat{Q}/C_l + T_p, \end{cases} \tag{15}$$

where $(\widehat{\cdot})$ represents the equilibrium value of the corresponding variable. A crucial simplification is obtained by assuming that the RTT is dominated by the propagation delay i.e., $Q(t)/C_l \ll T_p$, leading to the following system

$$\begin{cases} \dot{W}(t) = \frac{1}{T_p} - \frac{1}{2T_p} W(t)W(t-T_p)P(t-T_p), \\ \dot{Q}(t) = \frac{N}{T_p} W(t) - C_l. \end{cases} \tag{16}$$

This system can be further simplified using the time scaling proposed in [2], given by $t^{new} = t^{old}/T_p$. Therefore

$$\frac{dW}{dt^{old}} = \frac{dW}{dt^{new}} \frac{dt^{new}}{dt^{old}} = \frac{1}{T_p} \frac{dW}{dt^{new}}$$

and similarly, $dQ/dt^{old} = (dQ/dt^{new})/T_p$. Thus, system (16) becomes

$$\begin{cases} \dot{W}(t) = 1 - \frac{1}{2} W(t)W(t-1)P(t-1), \\ \dot{Q}(t) = NW(t) - C_l T_p \end{cases}$$

and defining new state variables as $w = W$ and $q = Q/N$ we obtain

$$\begin{cases} \dot{w}(t) = 1 - \frac{1}{2} w(t)w(t-1)P(t-1), \\ \dot{q}(t) = w(t) - c, \end{cases} \tag{17}$$

where $c := C_l T_p / N$ is the unique non dimensional parameter relating the physical ones.

Together with TCP, the congestion control is achieved with the AQM mechanism. In this sense, there are several approaches proposed in the literature and implemented in practice. Roughly speaking, the AQM scheme defines the way in which the probability $P(t)$ is computed based on some measure of variable $Q(t)$. In this paper, we will take three well-known schemes as study cases: the proportional (P) and proportional-integral (PI) compensators proposed in [6] and the widely used random early detection (RED).

4. Analysis of the different AQM strategies

4.1. Proportional control

For this scheme, the marking probability is made proportional to the queue length, i.e., $P(t) = KQ(t)$, where $K > 0$ is the controller gain. Several results concerning the nonlinear behavior of the resulting system can be found in [3,2,4]. In these articles, the authors performed a bifurcation analysis from different approaches: a combination of analytical and numerical tools [2], multiple scales method [3], and normal form and center manifold reductions [4]. Replacing with the proportional control $P(t - 1) = KQ(t - 1) = KNq(t - 1)$ in (17), we have

$$\begin{cases} \dot{w}(t) = 1 - kw(t)w(t-1)q(t-1)/2, \\ \dot{q}(t) = w(t) - c. \end{cases} \quad (18)$$

where $k := KN$. The details corresponding to the application of the FD approach can be found in the Appendix A.

A careful realization of system (18) allows to obtain the unique nonzero characteristic function

$$\hat{\lambda}(s; \mu) = (2s + kc^3)(e^{-s} - 1)/\chi(s), \quad (19)$$

where $\chi(s) =: 2cs^2 + 4s + kc^3$. As stated in Lemma 1, in order to determine Hopf bifurcations, we must take $s = i\omega$ and solve $\hat{\lambda}(i\omega_0; \mu_0) = -1$ for some values μ_0 and ω_0 . From this condition, the critical values of parameters can be expressed as functions of ω_0 as

$$(c_0, k_0) = \left(\frac{\cos \omega_0 + 1}{\omega_0 \sin \omega_0}, \frac{2\omega_0^4 \sin^4 \omega_0}{(1 + \cos \omega_0)^2} \right). \quad (20)$$

Taking ω_0 as a free parameter, we can obtain the Hopf curve in the (c, k) parameter space, as shown in Fig. 2(a). In this curve, the distinction between supercritical and subcritical bifurcations is achieved from the curvature coefficient given by (30). Noticeably, the bifurcation is supercritical over the whole curve. In addition, it is possible to compute the approximate amplitude of the emerging orbits, varying one parameter and keeping the other fixed, through the iterative procedure described in (11). The vector involved in this method is $\xi(i\omega; \mu) = -2cp_1(\omega; \mu)/\chi(i\omega)$, where the expression of $p_1(\omega; \mu)$ is given in (29). For example, in Fig. 2(b) we plot the amplitude ($\max\{w(t)\}$) vs. k for $c = 1$. Also we plot the same branch computed with DDE-BIFTOOL. The error in the predicted amplitude is due to the second-order harmonic balance used. These results can be improved using higher-order formulae as given in [10].

It has been found that increasing k beyond the Hopf bifurcation curve, a period-doubling cascade occurs, leading finally to a chaotic behavior [2]. Chaotic motion has also been found in discrete-time models of TCP/AQM networks [13]. These results illustrate that great care should be exercised when deriving simplified models of time-delay systems. As example, in [3,4] the authors considered the model

$$\begin{cases} \dot{W}(t) = \frac{1}{T_p} - \frac{K}{2T_p} W^2(t)Q(t - T_p), \\ \dot{Q}(t) = \frac{N}{T_p} W(t) - C_q, \end{cases} \quad (21)$$

that results from system (16) assuming that the product $W(t)W(t - T_p) \simeq W^2(t)$ when $W(t) \gg 1$, i.e., neglecting the propagation delay in the average TCP window size. Although this model allows for an easier computation of the Hopf bifurcation

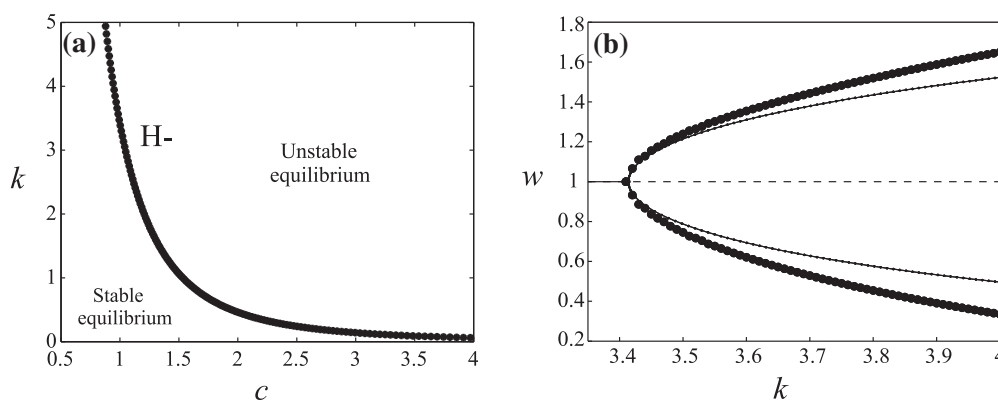


Fig. 2. (a) Hopf bifurcation curve for the system with proportional control. Label (H-) indicates a supercritical type. (b) One-parameter bifurcation diagram with $c = 1$. (-): stable equilibrium; (- -): unstable equilibrium point. For $k \simeq 3.41$ it bifurcates into a periodic solution. We plot the amplitude (maxima and minima of $w(t)$) on the cycles) computed with DDE-BIFTOOL (—) and approximated with the FD approach (•).

point, this simplification hides the chaotic nature of the system: using the Poincaré–Bendixon theorem for time-delay systems [14], it is possible to demonstrate that the model (21) does not exhibit chaotic behavior at all (the details can be found in the Appendix B and in [15]).

4.2. RED algorithm

As shown in [6], the RED controller is usually characterized by the transfer function

$$\frac{\Delta P(s)}{\Delta Q(s)} = \frac{KL}{s + K}, \tag{22}$$

where $\Delta P(s)$, $\Delta Q(s)$ are the Laplace transforms of $\delta P(t)$ and $\delta Q(t)$, respectively. These quantities represent small deviations around the equilibrium values they are defined as $\delta P(t) := P(t) - \hat{P}$ and $\delta Q(t) := Q(t) - \hat{Q}$. Notice that both time and variable Q are still not scaled. Constants K and L are proper parameters of the controller: K is the corner frequency in rad/s of the low-pass (averaging) filter, and L is the slope of the packet-marking profile implemented in the RED structure [5]. From (22), by applying the inverse Laplace transform, we obtain $\delta \dot{P}(t) + K\delta P(t) = KL\delta Q(t)$, and the dynamics of $P(t)$ results $\dot{P}(t) = -K[P(t) - \hat{P}] + KL[Q(t) - \hat{Q}]$. In the new time scale and from $Q(t) = Nq(t)$, this equation reads $\dot{P}(t) = -KT_p[P(t) - \hat{P}] + KLT_pN[q(t) - \hat{q}]$, so by choosing $p(t) := P(t)$, $k = KT_p$ and $\eta = KLT_pN$, the RED controlled model of the system is

$$\begin{cases} \dot{w}(t) &= 1 - w(t)w(t-1)p(t-1)/2, \\ \dot{q}(t) &= w(t) - c, \\ \dot{p}(t) &= -k[p(t) - \hat{p}] + \eta[q(t) - \hat{q}], \end{cases} \tag{23}$$

The vector of parameters is $\mu = (c, k, \eta)$, where c is system-dependent, k is controller-dependent, and η is both system and controller dependent.

As can be found in the Appendix A, a proper realization of system (23) allows to obtain the unique nonzero eigenvalue

$$\hat{\lambda}(s; \mu) = [2s(s+k) + \eta c^3](e^{-s} - 1)/\chi(s),$$

where $\chi(s) := 2cs^3 + 2(2+ck)s^2 + 4ks + \eta c^3$. As in the previous example, the critical condition given by Lemma 1 allows the computation of the Hopf curve, which is accomplished by detecting when the eigenvalue's locus passes through $-1 + i0$. Fig. 3(a) shows several Hopf curves, for different values of parameter η . For each case, the equilibrium's stability region is located to the left of the curve. Notice that η is proportional to the slope of the marking profile of RED strategy (L). Thus, as long as L increases, the stability region reduces. For small values of c , the rank of values of η for a stable equilibrium is relatively large. But, as pointed in [6], increasing values of c deteriorates stability, limiting the allowable values of η . On the other hand, the diagram in Fig. 3(b) shows the Hopf curves obtained for different values of k . The equilibrium is stable at the left of each curve. The value of k has a clear influence on the nature of the emerging periodic solutions. Increasing k not only enhances stability, but also forces the Hopf bifurcation to be supercritical over the whole curve, inhibiting the coexistence of unstable limit cycles with the stable equilibrium.

As a particular example, Fig. 4(a) shows the Hopf curve in the (c, k) parameter space for $\eta = 1$, where H- indicates *super-critical* bifurcations and H+ *subcritical* ones, according to the sign of σ_0 . This figure shows that in order to maintain the stability of the system, increasing values of parameter c (either because the channel capacity C_p is augmented or the number of TCP sessions N is reduced) must be accompanied by an increase of the bandwidth K of the controller. In addition, at the onset of the oscillating regime, the amplitude of the periodic solutions is approximated by using the auxiliary vector

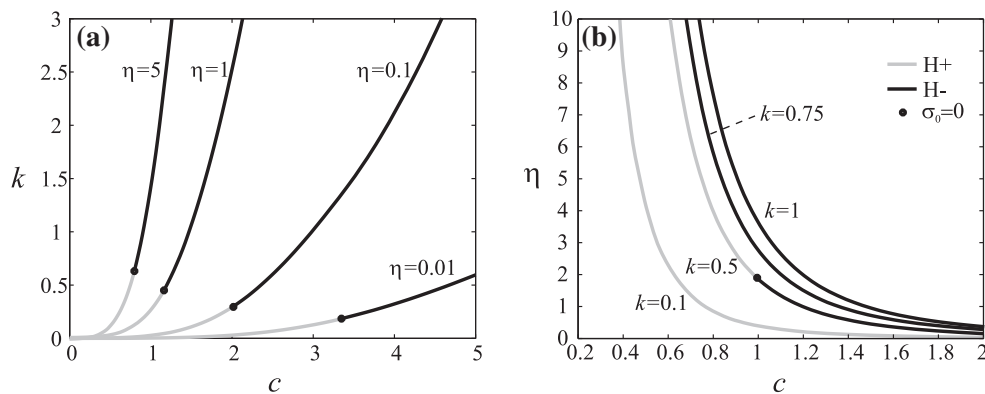


Fig. 3. (a) Hopf curves in the (c, k) space for several values of η . (b) Hopf bifurcation curves in the (c, η) plane for different values of k .

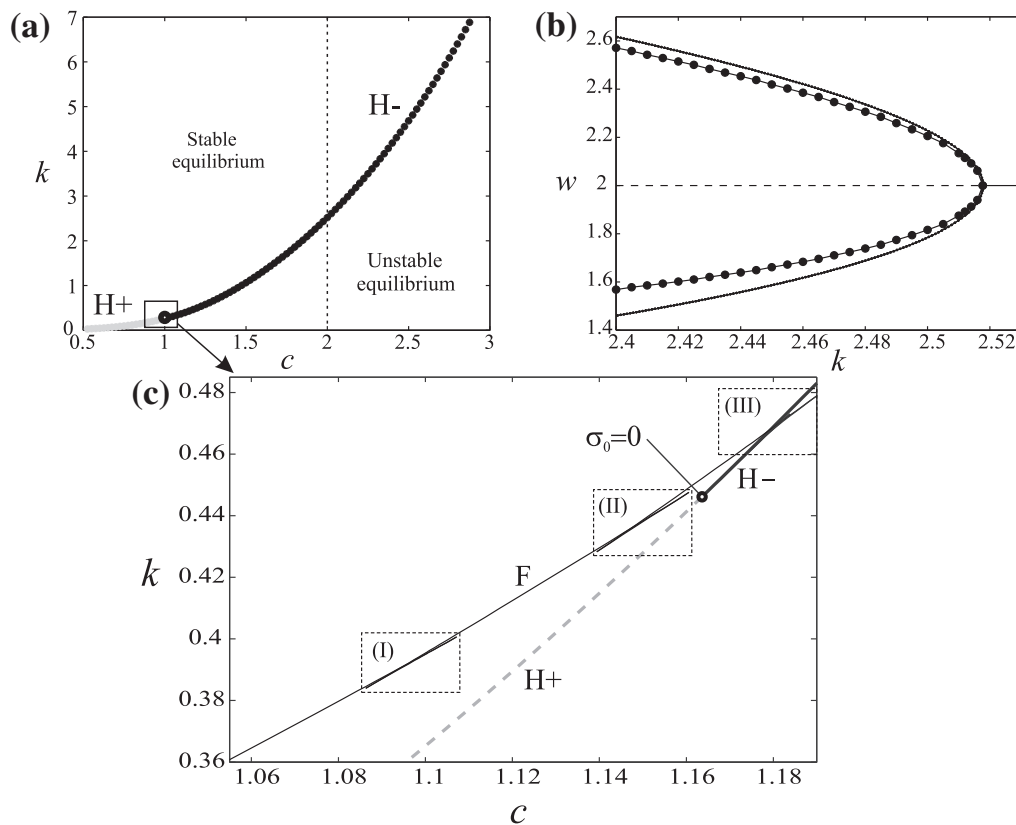


Fig. 4. (a) Hopf bifurcation curve for the system with RED control with $\eta = 1$. Note the curvature coefficient's failure point ($\sigma_0 = 0$) at $c \approx 1.165$ and $k \approx 0.448$. (b) One-parameter bifurcation diagram with $c = 2$. Stable equilibrium (—), unstable equilibrium (---), and branch of periodic solutions computed with DDE-BIFTOOL (·) and approximated with the FD approach (•). (c) Detail of the bifurcation diagram shown in (a), in a neighborhood of the point of failure ($\sigma_0 = 0$). Besides the Hopf subcritical (dashed line) and Hopf subcritical (heavy line) curves, it is shown the curve of fold of limit cycles (F, thin line).

$\xi(i\omega; \mu) = -2cp_1(\omega; \mu)/\chi(i\omega)$, where $p_1(\omega; \mu)$ is given by (33). Moreover, the stability of these solutions is verified by the curvature coefficient computed in (34).

The system with the RED controller exhibits a rich dynamic behavior. If the parameters (c, k) are close to the curve H+ in Fig. 4(a), the basin of attraction of \hat{y}^* is reduced because an unstable limit-cycle exists around the equilibrium point. On the other hand, if the parameters are close to the curve H– the system can be trapped in a stable oscillatory solution, such as the one represented in Fig. 4(b) for $c = 2$. This curve also shows the amplitude of the periodic solutions computed with a numerical tool (DDE-BIFTOOL, [12]) and the approximate solution given by the FD approach.

The presence of a degeneracy (labeled with $\sigma_0 = 0$ at $c \approx 1.165$ and $k \approx 0.448$), reveals the existence of folds of limit cycles in a neighborhood of this point (see [16]). This bifurcation consists of the annihilation of a couple of periodic solutions, and it can be detected when a Floquet multiplier of the corresponding orbit crosses the unit circle at the point $1 + i0$ (see [17]). This behavior is studied with the help of the DDE-BIFTOOL, and a detail of the curves of folds of limit-cycle bifurcations is shown in Fig. 4(c), labeled with F.

Three interesting scenarios appear in the zones indicated by the dashed boxes I, II and III in Fig. 4(c). A detailed view of box I is provided in Fig. 5(a), together with a qualitative diagram to clarify the regions with distinctive dynamic behavior in the parameter space. Up to four simultaneous periodic solutions can exist surrounding a stable equilibrium point: as an example, the amplitude of the periodic solutions emerging from the Hopf point as function of k for certain fixed values of c are shown in Fig. 5(b). As parameter c increases from $c = 1.0845$ (upper left) to $c = 1.1215$ (lower right), the following structural changes can be observed. First, a pair of fold points appear (F3-F6), originating a region of stable limit-cycles. A further increase in c causes that the fold point F6 approaches F7, until finally they collide annihilating the unstable oscillations of higher amplitude, as can be seen for $c = 1.1215$.

Box II has a similar qualitative dynamic behavior but for other range of values of parameters (c, k) . However, the behavior of the system for parameter values inside box III is different. A detailed view of this region is provided in Fig. 6(a), together with a qualitative diagram of the bifurcation curves. A maximum of five periodic orbits can appear, and their amplitudes for a range of values of parameter k and four fixed values of parameter c are represented in Fig. 6(b).

The oscillatory behavior commented above occurs in a rather small region of the (c, k) parameter space. Although it is probable that these regions are far from the normal operating point of actual systems, this analysis alerts of strange oscillatory behavior that may occur given the proper combination of parameters.

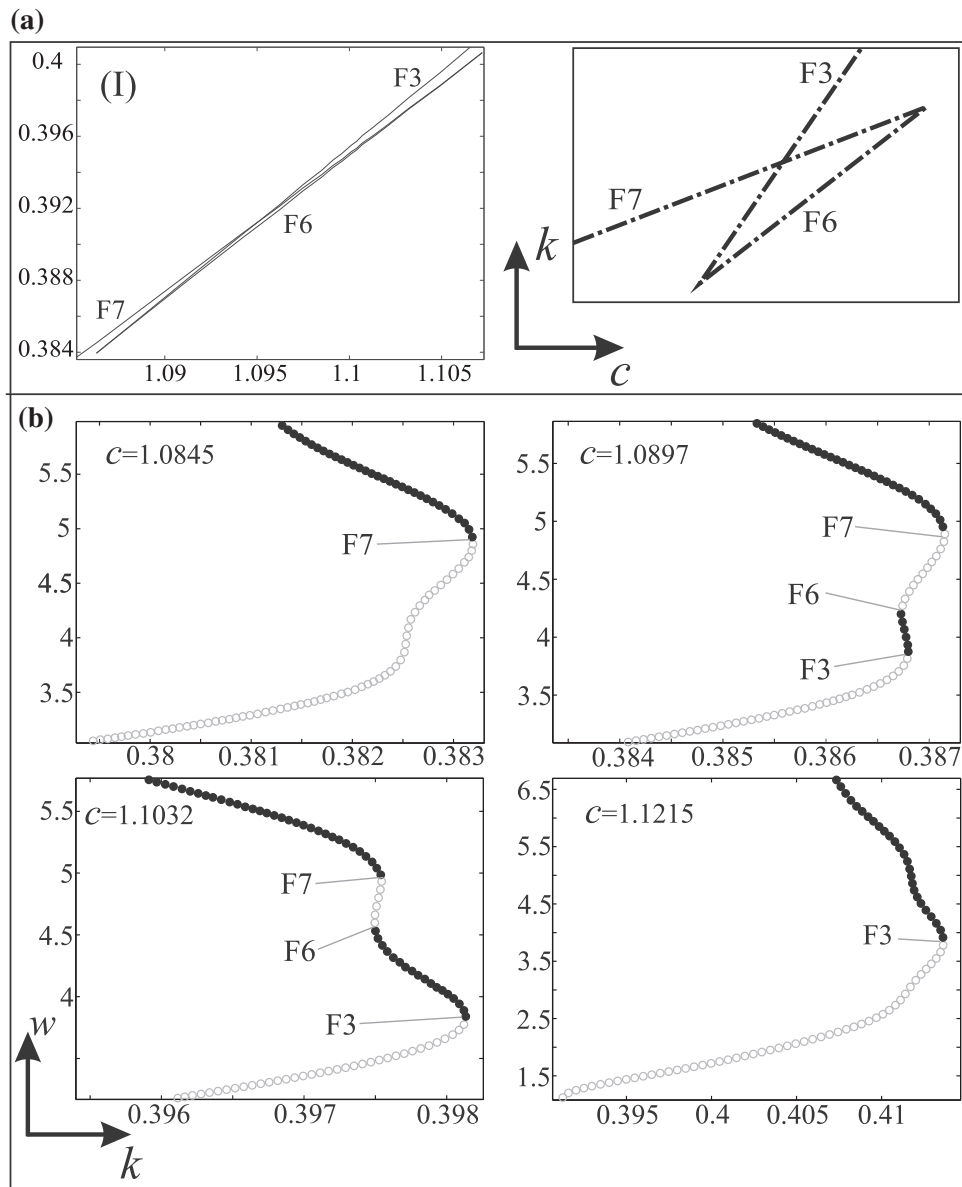


Fig. 5. (a) Left: Enlarged region corresponding to (I) in Fig. 4(c). Right: Qualitative diagram, which is similar for boxes I and II of Fig. 4(c). (b) Amplitude of periodic solutions vs. k , for several values of c corresponding to vertical cross section in (a). Notice the switching between stable (●) and unstable (○) limit cycles due to the fold bifurcations.

4.3. PI control

In this example, we deal with a controller with transfer function

$$\frac{\Delta P(s)}{\Delta Q(s)} = \frac{K}{s} \left(\frac{s}{z} + 1 \right), \tag{24}$$

where $\Delta P(s)$, $\Delta Q(s)$ are again the Laplace transforms of $\delta P(t)$ and $\delta Q(t)$ as in the previous example. Parameter K is the DC-gain and $z > 0$ sets the bandwidth of the PI compensator. From (24), it can be found that $\delta \dot{P}(t) = (K/z)\delta Q(t) + K\delta Q(t)$, and by changing the time scale and from $Q(t) = Nq(t)$, the dynamics of $P(t)$ can be expressed as

$$\begin{aligned} \dot{P}(t) &= (KN/z)\delta \dot{q}(t) + KNT_p \delta q(t) \\ &= (KN/z)[w(t) - c] + KNT_p \delta q(t). \end{aligned}$$

Then, by choosing $p(t) = P(t)$ and defining $\beta := KN/z$ and $\rho := KNT_p$, the PI controlled TCP/AQM model can be written as

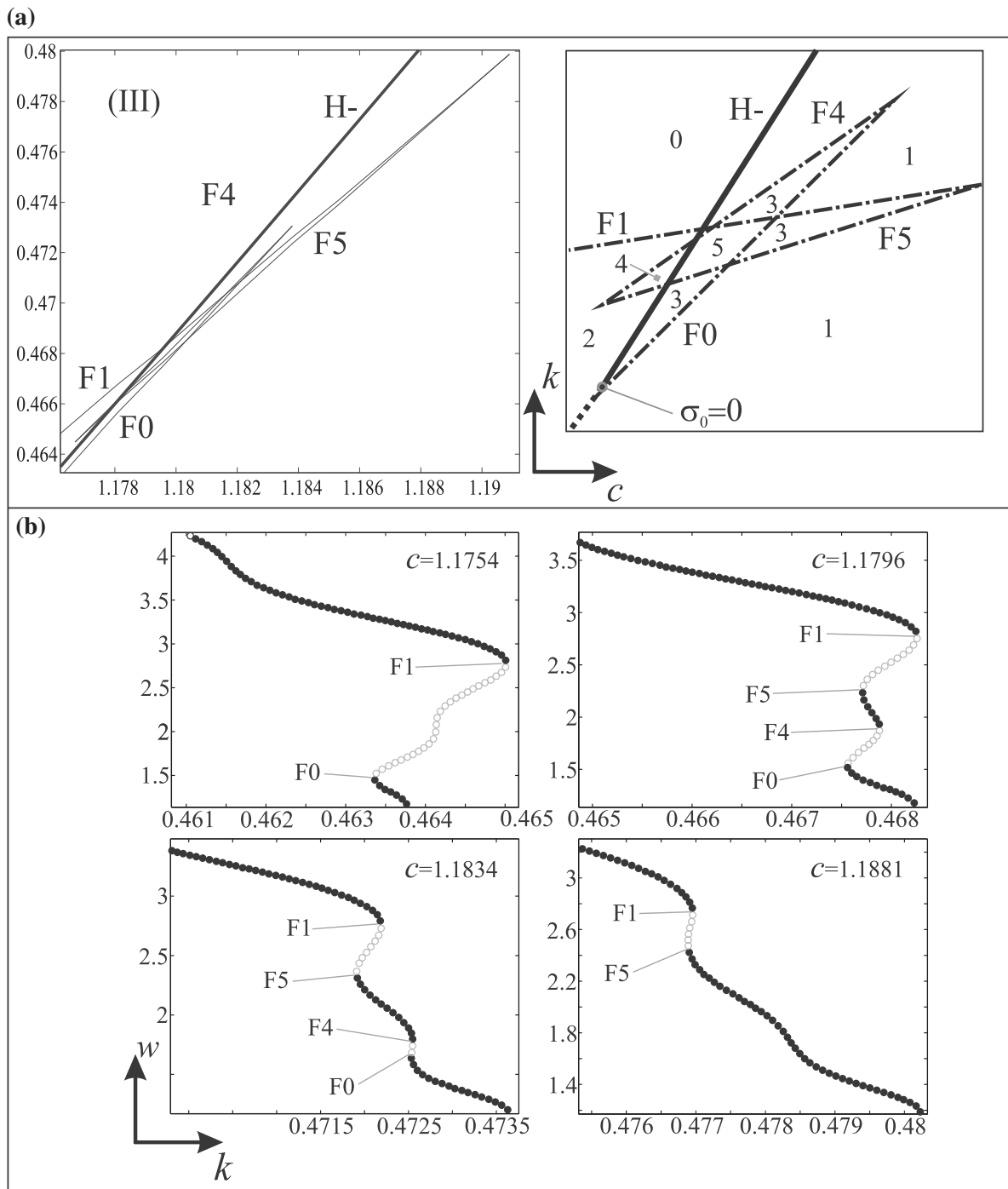


Fig. 6. (a) Left: Enlarged area corresponding to box (III) in Fig. 4(c). There are four fold curves near the Hopf one. Right: Qualitative sketch showing the shape of the singularity. The number in each region indicates the quantity of limit cycles. (b) Amplitude of periodic solutions vs. k , for several values of c , corresponding to vertical cross-sections of diagrams in (a). Stable (\bullet) and unstable (\circ) periodic orbits.

$$\begin{cases} \dot{w}(t) = 1 - w(t)w(t-1)p(t-1)/2, \\ \dot{q}(t) = w(t) - c, \\ \dot{p}(t) = \beta[w(t) - c] + \rho[q(t) - \hat{q}]. \end{cases} \quad (25)$$

Once again, we have three characterizing parameters, i.e., $\mu = (c, \beta, \rho)$. For this example, the relevant characteristic function results

$$\hat{\lambda}(s; \mu) = [2s^2 + c^3(\beta s + \rho)](e^{-s} - 1)/\chi(s),$$

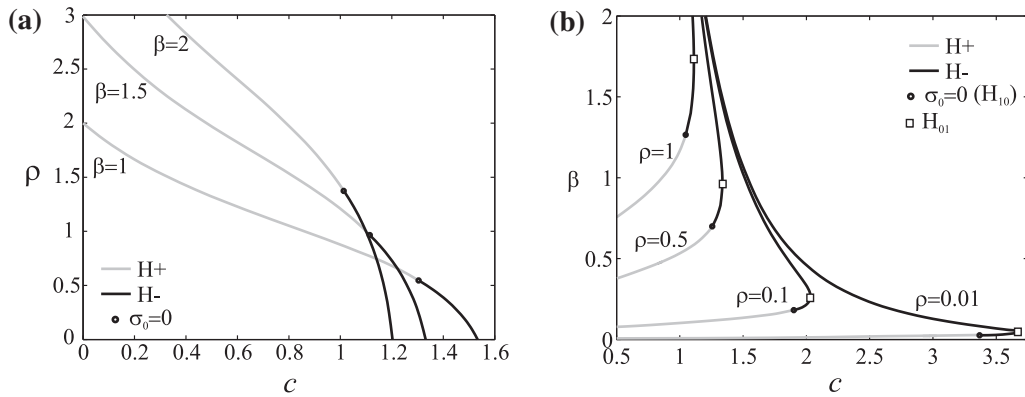


Fig. 7. (Left) Hopf curves in the (c, ρ) plane for several values of β . (Right) Hopf bifurcation curves in the (c, β) space for several values of ρ .

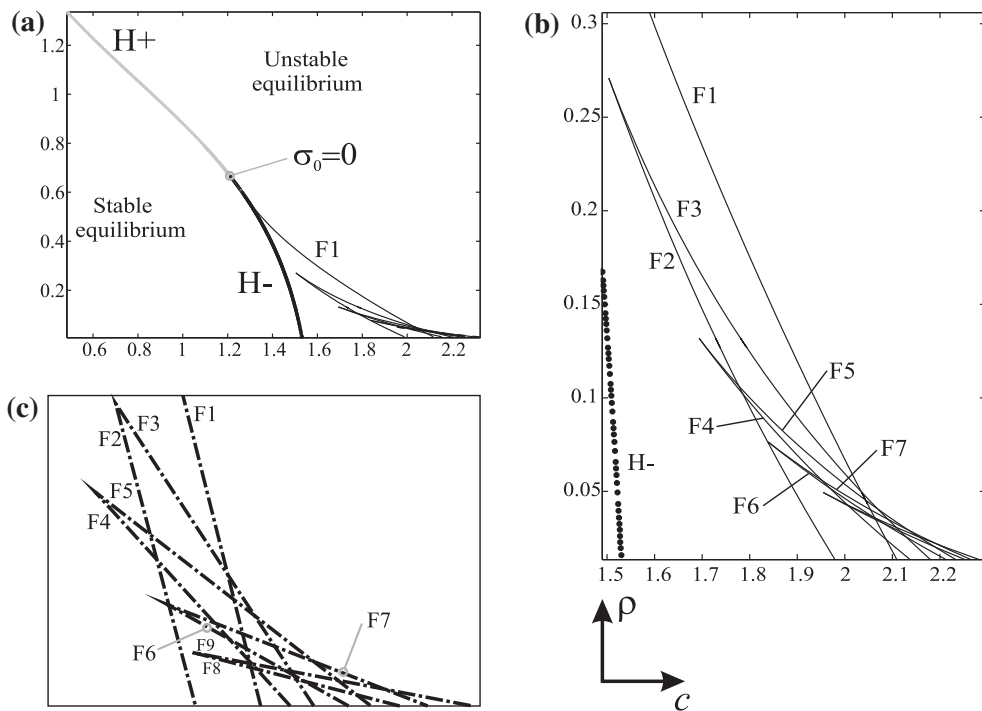


Fig. 8. (a) Bifurcation diagram for system with PI control. In the lower right corner there are several clustered fold curves. (b) Detail showing the curves of limit cycle-folds. The F1 originates at point of $\sigma_0 = 0$ at $(c, \rho) \approx (1.269, 0.594)$, as can be seen in (a). (c) Qualitative shape of the singularity. Notice that an horizontal cross-section can intersect up to nine folds.

where $\chi(s) := 2cs^3 + 4s^2 + c^3(s\beta + \rho)$ (see Appendix A). As in the previous examples, the characteristic locus allows to detect the combination of parameters that provokes Hopf bifurcations. Fig. 7(a) shows several Hopf curves in the (c, ρ) space for different values of β . The stability region lies below the corresponding Hopf curve. Notice the points in which the curvature coefficient vanishes, labeled with $\sigma_0 = 0$. For example, for $\beta = 1.5$, this degenerate Hopf point is at $(c, \rho) \approx (1.1150, 0.9675)$ and for $\beta = 2$, it is at $(c, \rho) \approx (1.0179, 1.3622)$. Fig. 7(b) shows several Hopf curves, for different values of ρ . In each case, the region at the left of the Hopf curve corresponds to a stable equilibrium. The points of failure of the curvature coefficient are indicated by small black dots. They are also frequently known as H_{10} , distinguishing them from those called H_{01} , which indicate degenerate Hopf bifurcations occurring when the transversality condition fails. This H_{01} degeneracy is detected when the characteristic locus arrives at point $-1 + i0$ with zero rate of change as the main bifurcation parameter varies. Mathematically, it is defined by condition $\partial \Re\{\lambda(i\omega_0; \mu)\} / \partial \mu = 0$. In the Hopf curves of Fig. 7(b), those points coincide with the rightmost extremes¹.

As mentioned before, the H_{10} degeneracy provokes the existence of folds of limit cycles. The points in the parameter space in which this phenomenon occurs can be continued with the help of the program DDE-BIFTOOL, as in the previous example.

¹ In the time domain formulation, this failure corresponds when a pair of complex conjugate eigenvalues with negative (positive) real part, first approach and reach the imaginary axis, and then enter the left (right) half plane again, as the parameter varies monotonically.

As a particular case of study, Fig. 8(a) shows the Hopf curve in the (c, ρ) parameter space for $\beta = 1$. Given that $c = C_l T_p / N$, if the propagation delay T_p increases, c increases (and also ρ), and the system can eventually become unstable. Similarly to the RED case (and contrary to intuition), increasing the link capacity C_l reduces the stability margin. The H_{10} degeneracy point ($\sigma_0 = 0$) is located at $(c, \rho) \approx (1.269, 0.594)$. From this point, a fold curve emerges, identified as F1 in Fig. 8(b). Also, in this figure, several fold curves appear. It is noticeably the way in which they organize, i.e., the shape of the whole singularity. This is depicted in the qualitative diagram of Fig. 8(c). Notice that for an horizontal cross-section, up to nine folds can be obtained. Perhaps this polycyclic behavior will be, in general, avoided in the practice by a proper compensator tuning. But if a variation in a key parameter leads the system to instability, multiple large amplitude oscillations can occur.

5. Conclusions

This work addresses the bifurcations arising in TCP/AQM systems. The choice of a proper AQM strategy should take into account the dynamical behavior that the system can have, which is not revealed by a linear model, or even a oversimplified nonlinear model, as shown in Section 4.1. In a system in which parameters are so variable, a bifurcation analysis seems to be rational when an AQM scheme is developed. Although several of such strategies are proposed in the literature, we only analyze three of them. They are representative and illustrate how the FD technique could be applied to other schemes. For the first example (P), we obtained results in agreement with [2]. For the RED and the PI controllers, we performed a bifurcation analysis which is novel at the best of our knowledge. We studied the feasibility of Hopf bifurcations and found the degeneracies associated with the failure of both the transversality condition and the curvature coefficient. Using numerical tools, global bifurcations such as folds of limit cycles, which lead to polycyclic configurations, were also detected. The knowledge of the dynamical scenarios (the bifurcation diagrams) may help to understand better how these control algorithms can be improved, a task that may be hard to accomplish using other approaches, for example, network simulations.

In addition, the FD technique allows to obtain approximations for the amplitude of the emerging periodic solutions, which actually represent the magnitude of fluctuations of the transmission rate.

A further improvement of these results could be accomplished by studying the border collision bifurcations, provoked by the finite capacity of links and the maximum window size allowed in the transmission (see [13]). However, this is out of the scope of the present study.

Acknowledgments

The financial support of the following grants is greatly appreciated: PICT 2010-0465 (ANPCyP), PIP 112-200801-01112 (CONICET) and PGI 24/K052 (UNS).

Appendix A

In the following, we provide the calculations leading to the results of Section 4. Notice that, in each example, choosing an adequate realization is essential in order to provide an easy computation of the Hopf bifurcation.

A.1. Proportional control (Section 4.1)

To apply the FD technique, system (18) must be rewritten in the feedback representation given by (1). In order to simplify calculations, we introduce constants a_1 and a_2 , whose values will be selected conveniently. We begin rewriting model (18) as

$$\begin{cases} \dot{w}(t) &= 1 - \frac{k}{2} w(t) w(t-1) q(t-1) - a_1 w(t) + a_1 w(t) - a_2 q(t) + a_2 q(t), \\ \dot{q}(t) &= w(t) - c. \end{cases} \tag{26}$$

Then, by choosing A, B, C and $\mathbf{g}(\mathbf{y}^*(t); \mu)$ as

$$\begin{aligned} A &= \begin{pmatrix} -a_1 & -a_2 \\ 1 & 0 \end{pmatrix}, \quad B = C = I_2, \quad F(e^{-s}) := \begin{pmatrix} I_2 \\ I_2 e^{-s} \end{pmatrix}, \\ \mathbf{g}(\mathbf{y}^*(t); \mu) &= \begin{pmatrix} 1 + \frac{k}{2} y_1(t) y_1(t-1) y_2(t-1) - a_1 y_1(t) - a_2 y_2(t) \\ -c \end{pmatrix}, \end{aligned} \tag{27}$$

where $(y_1(t), y_2(t)) = -(w(t), q(t))$, and system (26) can be rearranged as

$$\begin{pmatrix} \dot{w}(t) \\ \dot{q}(t) \end{pmatrix} = A \begin{pmatrix} w(t) \\ q(t) \end{pmatrix} + B \mathbf{g}(\mathbf{y}^*(t); \mu),$$

where $\mathbf{y}^*(t) = (y_1(t), y_2(t), y_1(t-1), y_2(t-1))^T$ is the extended output and $\mu = (c, k)$ represents the vector of parameters. From matrices given in (27), we have

$$G^*(s; \mu) := F(e^{-s})G(s; \mu) = \begin{pmatrix} G(s; \mu) \\ G(s; \mu)e^{-s} \end{pmatrix}, \quad G(s; \mu) = \frac{1}{\Delta(s)} \begin{pmatrix} s & -a_2 \\ 1 & s + a_1 \end{pmatrix},$$

where $\Delta(s) := s^2 + a_1s + a_2$. The equilibrium is computed from Eq. (2), resulting in $\hat{\mathbf{y}}^* = (-c, -2/(kc^2), -c, -2/(kc^2))$. Function $\mathbf{g}(\cdot)$ is linearized at this point and the following Jacobian results

$$J(\boldsymbol{\mu}) = \begin{pmatrix} \frac{k}{2}\hat{y}_1\hat{y}_2 - a_1 & -a_2 & \frac{k}{2}\hat{y}_1\hat{y}_2 & \frac{k}{2}(\hat{y}_1)^2 \\ 0 & 0 & 0 & 0 \end{pmatrix},$$

then for simplicity we choose $a_1 = k\hat{y}_1\hat{y}_2 = 2/c$, $a_2 = \frac{k}{2}(\hat{y}_1)^2 = kc^2/2$. This selection of a_1 and a_2 allows to derive a convenient expression of $\lambda(s; \mu)$. From $J(\boldsymbol{\mu})$ above, it follows that $G^*(s; \mu)J(\boldsymbol{\mu})$ has rank 1, and the only nonzero characteristic function is

$$\hat{\lambda}(s; \boldsymbol{\mu}) = (2s + kc^3)(e^{-s} - 1)/\chi(s), \tag{28}$$

where $\chi(s) := 2cs^2 + 4s + kc^3$. Then, the selection of a_1 and a_2 also ensures that the poles of $\hat{\lambda}(s; \boldsymbol{\mu})$ belong to the right-half plane (as can be easily verified), facilitating the stability analysis by means of Theorem 1. As stated in Lemma 1, we must take $s = i\omega$ and solve $\hat{\lambda}(i\omega_0; \boldsymbol{\mu}_0) = -1$ for some critical values $\boldsymbol{\mu}_0$ and ω_0 . This leads to

$$\begin{cases} k_0c_0^3 \cos \omega_0 + 2\omega_0 \sin \omega_0 & = 2c_0\omega_0^2, \\ -k_0c_0^3 \sin \omega_0 + 2\omega_0 \cos \omega_0 & = -2\omega_0 \end{cases}$$

and the critical values of parameters are expressed as functions of ω_0 as in (20). The right and left eigenvectors of $G^*(s; \mu)J(\boldsymbol{\mu})$ associated to $\hat{\lambda}(s; \boldsymbol{\mu})$ are $\mathbf{v} = (s, 1, se^{-s}, e^{-s})^T$, $\mathbf{u} = (-1, -kc^3/2, 1, kc^3/2)^T$, and from (7), matrices Q and L result in

$$Q = -\frac{e^{-s}}{2c^2} \begin{pmatrix} 2 + kc^3/s & 0 & 2 + kc^3 & kc(e^s + 1) \\ 0 & 0 & 0 & 0 \end{pmatrix}, \quad L = k\frac{e^{-s}}{s} \begin{pmatrix} e^{-s} & 0 & 1 & s \\ 0 & 0 & 0 & 0 \end{pmatrix}.$$

Also, we have

$$H^*(s; \mu) = \begin{pmatrix} H(s; \mu) \\ H(s; \mu)e^{-s} \end{pmatrix}, \quad H(s; \mu) = \frac{1}{\varphi(s)} \begin{pmatrix} 2cs & -kc^3 \\ 2c & 2[1 + e^s(1 + sc)] \end{pmatrix},$$

where $\varphi(s) := 2ce^s s^2 + 2(1 + e^s)s + kc^3$. From (6), we obtain

$$\mathbf{V}_{02} = v_0(\omega)(0, 1, 0, 1)^T, \quad \mathbf{V}_{22} = v_2(\omega)(i2\omega, 1, i2\omega e^{-i2\omega}, e^{-i2\omega})^T,$$

where

$$\begin{aligned} v_0(\omega) &:= -e^{-i\omega}[kc^4 - kc^3 e^{i\omega}(1 - i\omega + e^{i\omega}) + i2\omega(c + e^{i2\omega})]/[4kc^4], \\ v_2(\omega) &:= e^{-i2\omega}[kc^3(1 + i\omega) + (1 + c)(kc^3 + i2\omega)e^{i\omega}]/[2c\varphi(i2\omega)]. \end{aligned}$$

Thus, it results $\mathbf{p}(i\omega; \mu) = (p_1(\omega; \mu), 0)^T$, where

$$\begin{aligned} p_1(\omega; \mu) &:= e^{-i2\omega} \left\{ kc^2(2c^2v_2e^{i3\omega} - 1) - i8\omega v_2(1 + ce^{i3\omega}) \right. \\ &\quad \left. - 2kc^3[2v_0e^{i2\omega} + v_2 + e^{i\omega}(2v_0 + v_2(1 + i2\omega))] \right\} / 8c^2. \end{aligned} \tag{29}$$

Finally, it is obtained $\xi(i\omega; \mu) = -2cp_1(\omega; \mu)/\chi(i\omega)$. In addition, the curvature coefficient is given by

$$\sigma_0 = \Re \left\{ 2cp_1(\omega_0; \mu) / \left[1 + \left(1 + kc^3/2 + i\omega_0(1 + 2c) \right) e^{-i\omega_0} \right] \right\}. \tag{30}$$

A.2. Random early detection (RED) control (Section 4.2)

For the FD analysis of system (23), let us consider the following matrices

$$\begin{aligned} A &= \begin{pmatrix} -a_1 & 0 & -a_2 \\ 1 & 0 & 0 \\ 0 & \eta & -k \end{pmatrix}, \quad B = I_3, \quad C = \begin{pmatrix} 1 & 0 & 0 \\ 0 & 0 & 1 \end{pmatrix}, \quad F(e^{-s}) := \begin{pmatrix} I_2 \\ I_2 e^{-s} \end{pmatrix}, \\ \mathbf{g}(\mathbf{y}^*(t); \boldsymbol{\mu}) &= \begin{pmatrix} 1 + \frac{1}{2}y_1(t)y_1(t-1)y_2(t-1) - a_1y_1(t) - a_2y_2(t) \\ -c \\ k\hat{p} - \eta\hat{q} \end{pmatrix}. \end{aligned} \tag{31}$$

Notice that we have introduced auxiliary constants a_1 and a_2 as in the previous example. The transfer function for the linear part is given by

$$G^*(s; \mu) = \begin{pmatrix} G(s; \mu) \\ G(s; \mu)e^{-s} \end{pmatrix}, \quad G(s; \mu) = \frac{1}{\Delta(s)} \begin{pmatrix} s(s+k) & -a_2 & -a_2s \\ 1 & s+a_1 & s(s+a_1) \end{pmatrix},$$

where $\Delta(s) := s^3 + (a_1 + k)s^2 + a_1ks + \eta a_2$. By defining $a_1 = \eta \hat{y}_1 \hat{y}_2 = 2/c$ and $a_2 = (\hat{y}_1)^2/2 = c^2/2$, the Jacobian results in

$$J(\mu) = \begin{pmatrix} -1/c & -c^2/2 & 1/c & c^2/2 \\ 0 & 0 & 0 & 0 \\ 0 & 0 & 0 & 0 \end{pmatrix}. \tag{32}$$

As $\text{rank}\{G^*(s; \mu)J(\mu)\} = 1$, the unique nonzero eigenvalue is

$$\hat{\lambda}(s; \mu) = [2s(s+k) + \eta c^3](e^{-s} - 1)/\chi(s),$$

where $\chi(s) := 2cs^3 + 2(2 + ck)s^2 + 4ks + \eta c^3 = 2c\Delta(s)$. Eigenvectors \mathbf{v} and \mathbf{u} of matrix $G^*(s; \mu)J(\mu)$ are $\mathbf{v} = (s(s+k), \eta, s(s+k)e^{-s}, \eta e^{-s})^T$, $\mathbf{u} = (-1, -c^3/2, 1, c^3/2)^T$, and matrices Q and L result in

$$Q = \begin{pmatrix} q_{11}(s) & 0 & q_{13}(s) & q_{14}(s) \\ 0 & 0 & 0 & 0 \\ 0 & 0 & 0 & 0 \end{pmatrix}, \quad L = s(s+k)e^{-s} \begin{pmatrix} \eta e^{-s} & 0 & \eta & -s(s+k) \\ 0 & 0 & 0 & 0 \\ 0 & 0 & 0 & 0 \end{pmatrix},$$

where $q_{11}(s) := -[2s(s+k) + \eta c^3]e^{-s}/2c^2$, $q_{13}(s) := -[2s(s+k) + \eta c^3 e^{-s}]/2c^2$ and $q_{14}(s) := -cs(s+k)(1 + e^{-s})/2$. The closed-loop transfer function reads

$$H^*(s; \mu) = \begin{pmatrix} H(s; \mu) \\ H(s; \mu)e^{-s} \end{pmatrix}, \quad H(s; \mu) = \frac{1}{\varphi(s)} \begin{pmatrix} 2cs(s+k) & -\eta c^3 & -c^3s \\ 2c\eta & 2\eta\vartheta(s) & 2s\vartheta(s) \end{pmatrix},$$

where $\vartheta(s) := 1 + e^s(1 + cs)$ and $\varphi(s) := 2s(s+k)\vartheta(s) + \eta c^3$. Vectors \mathbf{V}_{02} and \mathbf{V}_{22} are obtained as

$$\mathbf{V}_{02} = v_0(\omega)(0, -1, 0, -1)^T, \quad \mathbf{V}_{22} = v_2(\omega)(v_1^{22}, \eta/2, v_1^{22}e^{-i2\omega}, \eta e^{-i2\omega}/2)^T,$$

where $v_1^{22} := i\omega(k + i2\omega)$ and

$$v_0(\omega) := \omega \left\{ [\eta c^3 - 2(k^2 + \omega^2)]\omega \cos \omega + \eta c^3(\omega + k \sin \omega) \right\} / [2c^4],$$

$$v_2(\omega) := i\omega(k + i\omega)e^{-i2\omega} \left\{ \eta c^3 + e^{i\omega}[\eta c^3 + i2\omega(k + i\omega)] \right\} / [c\varphi(i2\omega)].$$

Then, we have $\mathbf{p}(i\omega; \mu) = (p_1(\omega; \mu), 0, 0)^T$, where

$$p_1 = \frac{\omega e^{-i2\omega}}{8c^2} \left\{ \eta c^2 \omega(\omega - ik)(\omega + ik + 2\omega e^{i2\omega}) - 4\omega v_2(1 + e^{i3\omega})(k^2 + ik\omega + 2\omega^2) \right. \\ \left. + ic^3 [v_2[(k - i\omega)(1 + e^{i\omega}) - 2\eta e^{i\omega}(k + i2\omega)(1 + e^{i2\omega})] \right. \\ \left. + 4v_0 e^{i\omega}(k + i\omega)(1 - e^{i\omega})] \right\}. \tag{33}$$

Thus, we compute $\xi(i\omega; \mu) = -2cp_1(\omega; \mu)/\chi(i\omega)$, and the curvature coefficient becomes

$$\sigma_0 = -2c \Re \left\{ p_1(\omega_0; \mu) / [q(\omega_0)e^{-i\omega_0} + \chi'(i\omega_0)] \right\}, \tag{34}$$

where $q(\omega) := 2\omega^2 - \eta c^3 + 2k(1 - e^{i\omega}) - i2\omega(k - 2 + 2e^{-i\omega})$.

A.3. Proportional-integral control (Section 4.3)

To apply the FD approach to system (25), let us consider the auxiliary constants a_1 and a_2 again and take the realization

$$A = \begin{pmatrix} -a_1 & 0 & -a_2 \\ 1 & 0 & 0 \\ \beta & \rho & 0 \end{pmatrix}, \quad B = I_3, \quad C = \begin{pmatrix} 1 & 0 & 0 \\ 0 & 0 & 1 \end{pmatrix}, \quad F(e^{-s}) := \begin{pmatrix} I_2 \\ I_2 e^{-s} \end{pmatrix}, \tag{35}$$

$$g(\mathbf{y}^*(t); \mu) = \begin{pmatrix} 1 + y_1(t)y_1(t-1)y_2(t-1)/2 - a_1y_1(t) - a_2y_2(t) \\ -c \\ -(\beta c + \rho \hat{q}) \end{pmatrix}.$$

For the linear part we have

$$G^*(s; \mu) = \begin{pmatrix} G(s; \mu) \\ G(s; \mu)e^{-s} \end{pmatrix}, \quad G(s; \mu) = \frac{1}{\Delta(s)} \begin{pmatrix} s^2 & -a_2\rho & -a_2s \\ \beta s + \rho & \rho(s+a_1) & s(s+a_1) \end{pmatrix},$$

where $\Delta(s) := s^3 + a_1s^2 + \beta a_2s + \rho a_2$. Also, by taking $a_1 = \widehat{y}_1\widehat{y}_2 = 2/c$ and $a_2 = (\widehat{y}_1)^2/2 = c^2/2$, the Jacobian results identical as for the RED case (see (32)). Again, $G^*(s; \mu)J(\mu)$ has rank 1, and the relevant eigenvalue reads

$$\widehat{\lambda}(s; \mu) = [2s^2 + c^3(\beta s + \rho)](e^{-s} - 1)/\chi(s),$$

where $\chi(s) := 2cs^3 + 4s^2 + \beta c^3s + \rho c^3$. It is possible to verify that the roots of $\chi(s)$ (the poles of $\widehat{\lambda}(s; \mu)$) belong to the left half plane. Eigenvectors \mathbf{v} and \mathbf{u} of $G^*(s; \mu)J(\mu)$ associated with $\widehat{\lambda}(s; \mu)$ are $\mathbf{v} = (s^2/(\beta s + \rho), 1, s^2e^{-s}/(\beta s + \rho), e^{-s})^T$, $\mathbf{u} = (-1, -c^3/2, 1, c^3/2)^T$, and matrices Q and L result

$$Q = \begin{pmatrix} q_{11} & 0 & q_{13} & q_{14} \\ 0 & 0 & 0 & 0 \\ 0 & 0 & 0 & 0 \end{pmatrix}, \quad L = \frac{s^2e^{-s}}{(\beta s + \rho)} \begin{pmatrix} e^{-s} & 0 & 1 & \frac{s^2}{(\beta s + \rho)} \\ 0 & 0 & 0 & 0 \\ 0 & 0 & 0 & 0 \end{pmatrix},$$

where $q_{11} = -\frac{e^{-s}}{2c^2} \left(\frac{2s^2}{\beta s + \rho} + c^3 \right)$, $q_{13} = -\frac{ce^{-s}}{2} - \frac{s^2}{c^2(\beta s + \rho)}$, $q_{14} = -\frac{s^2c(1+e^{-s})}{2(\beta s + \rho)}$.

Closed-loop matrix $H(s; \mu)$ is given by

$$H^*(s; \mu) = \begin{pmatrix} H(s; \mu) \\ H(s; \mu)e^{-s} \end{pmatrix}, \quad H(s; \mu) = \frac{1}{\varphi(s)} \begin{pmatrix} 2cs^2 & -\rho c^3 & -c^3s \\ 2c(\beta s + \rho) & 2\rho\vartheta(s) & 2s\vartheta(s) \end{pmatrix},$$

where $\vartheta(s) := 1 + e^s(1 + cs)$ and $\varphi(s) := 2s^2\vartheta(s) + c^3(\beta s + \rho)$. Thus we obtain

$$\mathbf{V}_{02} = v_0(\omega)(0, 1, 0, 1)^T,$$

$$\mathbf{V}_{22} = v_2(\omega)(2\omega^2, -(\rho + i2\omega\beta)/2, 2\omega^2e^{-i2\omega}, -(\rho + i2\omega\beta)/2e^{-i2\omega})^T,$$

where

$$v_0(\omega) := -\omega^2 [(\rho c^3 - 2\omega^2) \cos \omega + c^3(\rho + \beta\omega \sin \omega)] / [2c^4(\rho^2 + \omega^2\beta^2)],$$

$$v_2(\omega) := \omega^2 e^{-i2\omega} [e^{i\omega}(\rho c^3 - 2\omega^2 + ic^3\beta\omega) + c^3(\rho + i\omega\beta)] / [c\varphi(i2\omega)(\rho + i\omega\beta)^2].$$

Then, we compute $\mathbf{p}(i\omega; \mu) = (p_1(\omega; \mu), 0, 0)^T$, where

$$p_1 = \frac{i\omega^2 e^{-i2\omega}}{8c^2(\rho^2 + \omega^2\beta^2)(\rho + i\omega\beta)} \left\{ c^2\omega^2(\omega\beta + \rho(1 + 2e^{i2\omega})) - i8\omega^2v_2(1 + e^{i3\omega})(\rho + i\omega\beta)^2 + ic^3(\rho + i\omega\beta)[-4v_0(\rho - i\omega)e^{i\omega}(1 + e^{i\omega}) + v_2[\rho^2(1 + 5e^{i\omega} + 4e^{i3\omega}) + \omega^2\beta^2(e^{i\omega} + 4e^{i3\omega} - 2) + i3\omega\beta\rho(1 + e^{i\omega})]] \right\}. \tag{36}$$

Also, we have $\xi(i\omega; \mu) = -2c(\rho + i\omega\beta)p_1(\omega; \mu)/\chi(i\omega)$, and finally

$$\sigma_0 = -2c \Re \{ (\rho + i\omega_0\beta)p_1(\omega_0; \mu) / [q(\omega_0)e^{-i\omega_0} + \chi'(i\omega_0)] \}, \tag{37}$$

where $q(\omega) := 2\omega^2 - i\omega(4e^{i\omega} - 4 + \beta c^3) - c^3[\rho + \beta(e^{i\omega} - 1)]$.

Appendix B

Here we will follow the presentation given in [15]. Let us consider

$$\begin{cases} \dot{x}_i(t) &= f_i(x_i(t), x_{i+1}(t - r_i)), \quad 1 \leq i \leq N - 1, \\ \dot{x}_N(t) &= f_N(x_N(t), x_1(t - r_N)), \end{cases} \tag{38}$$

where $r_i \geq 0$, $f_i \in C^1$ and $\partial f_i(x, y)/\partial y \neq 0$, $\forall (x, y) \in \mathbb{R}^2$, $1 \leq i \leq N - 1$. Notice that the evolution of x_1 is influenced by x_2 , which is influenced by x_3 , and so on, until finally x_N is influenced by x_1 . Systems of this special kind have been studied in [14] and they are called MCFS (“monotone cyclic feedback systems”). If $\mathbf{x}(t)$ is a periodic solution of (38), then $\mathbf{z} \in \mathbb{R}^n$ is called a *limit point* of this solution if there is a sequence $\{t_k\}$ in \mathbb{R}^+ such that $t_k \rightarrow \infty$ and $\mathbf{x}(t_k) \rightarrow \mathbf{z}$. The set of all limit points of $\mathbf{x}(t)$ is called its Ω -*limit set* and is denoted by $\Omega(\mathbf{x})$. Also, suppose that \widehat{X} is the set of all equilibria of (38). Then, we have the following result developed in [14], which is presented conveniently as follows:

Theorem 2. *If $\mathbf{x}(t)$ is a bounded solution of MCFS (38) on $[t_0, +\infty)$, then*

- (a) $\Omega(\mathbf{x})$ is a nonconstant periodic orbit, or
- (b) The Ω -limit set of every solution $\mathbf{s}(t)$, defined for $t \geq 0$ with $\mathbf{s}(t + \theta) \in \Omega(\mathbf{x})$, $-\max\{r_i\} \leq \theta \leq 0$, is contained in \widehat{X} .

Point (b) takes into account the case when $\Omega(\mathbf{x})$ is a single equilibrium point. It is interesting to note that this theorem rules out chaotic solutions on system (38) (see [15]). Taking into account system (21), by a suitable variable scaling, it is rewritten as

$$\begin{cases} \dot{w}(t) &= 1 - kw^2(t)q(t-1)/2, \\ \dot{q}(t) &= w(t) - c, \end{cases} \quad (39)$$

where c and k have the same definitions as in (18). Then, system (39) is a MCFS, with $N = 2$ and $f_1(x, y) = 1 - kx^2y/2$, $f_2(x, y) = x - c$, where $r_1 = 1, r_2 = 0$ and also $\partial f_1(x, y)/\partial y = -kx^2/2$, $\partial f_2(x, y)/\partial y = 1$. Notice that $\partial f_1(x, y)/\partial y$ is not zero by assuming positive values of x , which has sense because $w(t)$ (the average window size) is assumed to be positive. Thus, according to Theorem 2, the simplified system (39) cannot present chaotic behavior.

References

- [1] Li C, Chen G, Liao X, Yu J. Hopf bifurcation in an internet congestion control model. *Chaos Solitons Fractals* 2004;19:853–62.
- [2] Michiels W, Niculescu SI. Stability analysis of a fluid flow model for TCP like behavior. *Int J Bifurcation Chaos* 2005;15:2277–82.
- [3] Ding D, Zhu J, Luo X. Hopf bifurcation analysis in a fluid flow model of internet congestion control algorithm. *Nonlinear Anal Real World Appl* 2009;10:824–39.
- [4] Zheng YG, Wang ZH. Stability and Hopf bifurcation of a class of TCP/AQM networks. *Nonlinear Anal Real World Appl* 2010;11:1552–9.
- [5] Misra V, Gong W, Towsley D. Fluid-based analysis of a network of AQM routers supporting TCP flows with an application to RED. In: Presented at the proceedings of ACM/SIGCOMM; 2000.
- [6] Hollot CV, Misra V, Towsley D, Gong W. Analysis and design of controllers for AQM routers supporting TCP flows. *IEEE Trans Autom Control* 2002;47:945–59.
- [7] Raina G, Heckmann O. TCP: local stability and Hopf bifurcation. *Performance Eval* 2007;64:266–75.
- [8] Mees AI, Chua LO. The Hopf bifurcation theorem and its applications to nonlinear oscillations in circuits and systems. *IEEE Trans Circuits Syst* 1979;4:235–54.
- [9] Mees AI. Dynamics of feedback systems. Chichester, UK: John Wiley & Sons; 1981.
- [10] Moiola JL, Chen G. Hopf bifurcation analysis: a frequency domain approach. Singapore: World Scientific Publishing Co.; 1996.
- [11] Gentile FS, Moiola JL, Paolini EE. On the study of bifurcations in delay-differential equations: a frequency-domain approach. *Int J Bifurcation Chaos* 2012;22:1250137.
- [12] Engelborghs K, Luzyanina T, Samaey G, DDE-BIFTOOL V. 2.00: a Matlab package for bifurcation analysis of delay differential equations, typeTW report 330, Department of Computer Science, Katholieke Universiteit Leuven, Belgium; 2001.
- [13] Ranjan P, Abed EH, La RJ. Nonlinear instabilities in TCP-RED. *IEEE Trans. Networking* 2004;12:1079–92.
- [14] Mallet-Paret J, Sell GR. The Poincaré–Bendixson theorem for monotone cyclic feedback systems with delay. *J Differ. Equ.* 1996;125:441–89.
- [15] Smith H. An introduction to delay differential equations with applications to the life sciences. Springer; 2010.
- [16] Kuznetsov YA. Elements of applied bifurcation theory. 3rd ed. New York: Springer-Verlag; 2004.
- [17] Seydel R. Practical bifurcation and stability analysis. 3rd ed. Springer; 2010.